Available online at www.sciencedirect.com
ScienceDirect
Comput. Methods Appl. Mech. Engrg. 283 (2015) 280–302
www.elsevier.com/locate/cma

A coupled Eulerian–Lagrangian extended finite element formulation for simulating large deformations in hyperelastic media with moving free boundaries

Louis Foucard[a], Anup Aryal[b], Ravindra Duddu[b,*], Franck Vernerey[a,*]

[a] Department of Civil, Environmental and Architectural Engineering, Program of Mechanical Science and Engineering, University of Colorado, Boulder, United States
[b] Department of Civil and Environmental Engineering, Vanderbilt University, Nashville, TN, United States

Received 1 May 2014; received in revised form 10 September 2014; accepted 14 September 2014
Available online 2 October 2014

Abstract

We present a coupled Eulerian–Lagrangian (CEL) formulation aimed at modeling the moving interface of hyperelastic materials undergoing large to extreme deformations. This formulation is based on an Eulerian description of kinematics of deformable bodies together with an updated Lagrangian formulation for the transport of the deformation gradient tensor. The extended finite element method (XFEM) is used to discretize the mechanical equilibrium and deformation gradient transport equations in a two-phase domain. A mixed interpolation scheme (biquadratic for the velocity and bilinear for the deformation gradient) is adopted to improve the accuracy of the numerical formulation. The interface describing the deformed shape of the body is represented by the level set function and is evolved using the grid based particle method. The performance of the scheme is explored in two-dimensions in the compressible regime. For an adequate spatial and temporal discretization, our numerical results are in good agreement with theory and with numerical results from the traditional Lagrangian formulation (in Abaqus). The advantage of the proposed formulation is that material motion is not coupled with that of the mesh; this eliminates the issues of mesh distortion and the need for remeshing associated with Lagrangian formulations when bodies undergo very large distortions. It is therefore well adapted to describe the motion of complex fluids and soft matter whose physical properties are intermediate between conventional liquids and solids.

Keywords: Non-linear elasticity; Large deformation; Moving interface; XFEM and level sets; Mixed element formulation; Eulerian solid mechanics

1. Introduction

Many important and challenging problems in the areas of geophysics (e.g. ice sheet flow, mantle dynamics), soft materials (e.g. deformation of hydrogels and biological cells) and material science (e.g. metal forming) involve large

* Correspondence to: Department of Civil and Environmental Engineering, Vanderbilt University, Rm# 274 Jacobs Hall, 400 24th Avenue South, 37212 Nashville, TN, United States. Tel.: +1 615 343 4891.
* Correspondence to: Department of Mechanical Engineering, University of Colorado Boulder, ECME 124, 1111 Engineering Drive, Boulder, CO, 80309-0428, United States. Tel.: +1 303 492 7165.
E-mail addresses: duddu@gmail.com, ravindra.duddu@vanderbilt.edu (R. Duddu), franck.vernerey@colorado.edu (F. Vernerey).

http://dx.doi.org/10.1016/j.cma.2014.09.016
0045-7825/

deformations or ow of solid material. In these conditions, it can be convenient to work with a fully Eulerian description of solid deformation, especially when the boundaries of the solid domain are not moving [1,2]. For problems where domain boundaries are free to move, however, a Lagrangian (material) description is required to map solid deformation between reference and current con gurations. Such a moving boundary problem also needs the introduction of specialized numerical methods that can track an interface without remediating to expensive remeshing techniques. In this context, we propose to address the challenges with describing the evolution of free boundaries

equation in an Eulerian framework, and is then used to update the isochoric and volumetric parts of the deformation gradient, separately, using an updated Lagrangian description. The position of the material interface is tracked using the GPM [3] and the velocity field projected in the direction normal to the interface. We show that the method is accurate in the regime of finite deformation and viable for investigating soft matter mechanics. The organization of the paper is as follows: Section 2 introduces the kinematics, the governing and constitutive equations, and the resulting weak form for the mechanical equilibrium of an elastic body. In Section 3, we present a numerical strategy to discretize the weak form, the tracking of the interface and the Lagrangian transport of the deformation gradient tensor components. Finally, the numerical convergence and accuracy of the method are demonstrated in Section 4 through the examples of a uniaxial extension of a rectangular bar, and the simple shear of a rectangular block. The mesh-independent geometric discretization and the absence of mesh distortion problem is then demonstrated with the test of a cylinder under compression and the indentation of a rectangular block. The latter results are validated by comparing them with those from traditional Lagrangian formulation in the commercial software Abaqus. Some concluding remarks are made in Section 5.

2. Formulation of the governing equations

2.1. Kinematics

In this study we consider a domain Ω containing an elastic body in the region $\Omega^s(t)$. The domain Ω is delimited by a boundary $\partial\Omega$ while the interface describing the current shape of the elastic body is denoted by $\Gamma(t)$. Thus, Γ splits the domain Ω into the solid domain $\Omega^s(t)$ and its complement denoted by $\Omega^n(t)$. We employ the Eulerian description of the motion and choose a fixed right-handed Cartesian system of coordinates $\{O; \mathbf{e}_j;\ j = 1, 2, 3\}$, where $\mathbf{e}_j$ are the orthonormal basis vectors [33]. The motion of a physical particle P is expressed by the mapping function $\mathbf{x} = \boldsymbol{\chi}(\mathbf{X}, t)$ between its reference coordinates $\{\mathbf{X} = X_j\,\mathbf{e}_j;\ j = 1, 2, 3\}$ at an initial time t

$$/,$$

where $\bar{\mathbf{b}} = \bar{\mathbf{F}}\bar{\mathbf{F}}^T = J^{-2/3}\mathbf{F}\mathbf{F}^T$. The specific functional forms of U and $\hat{W}$ are to be chosen to satisfy physical conditions. Herein, we assume the functions proposed by Simo et al. [34,35] as,

$$\begin{aligned} U(J) &= \frac{\kappa}{2}\left[\ln(J)\right]^2; \\ \hat{W}(\bar{\mathbf{b}}) &= \frac{\mu}{2}\left[\operatorname{tr}(\bar{\mathbf{b}}) - 3\right]; \end{aligned} \tag{14}$$

where μ and κ represent the shear and bulk modulus of the material, respectively, and `tr' denotes the trace of the tensor and $\bar{\mathbf{b}} = \bar{\mathbf{F}}\bar{\mathbf{F}}^T$. The expression for the Cauchy stress is [2],

$$\boldsymbol{\sigma}(J, \bar{\mathbf{F}}) = \frac{1}{J}\left[\kappa \ln(J)\mathbf{I} + \operatorname{dev}(\bar{\mathbf{b}})\right] \tag{15}$$

where $\operatorname{dev}(\bar{\mathbf{b}}) = \bar{\mathbf{b}} - \frac{1}{3}\operatorname{tr}(\bar{\mathbf{b}})\mathbf{I}$ is deviatoric part.

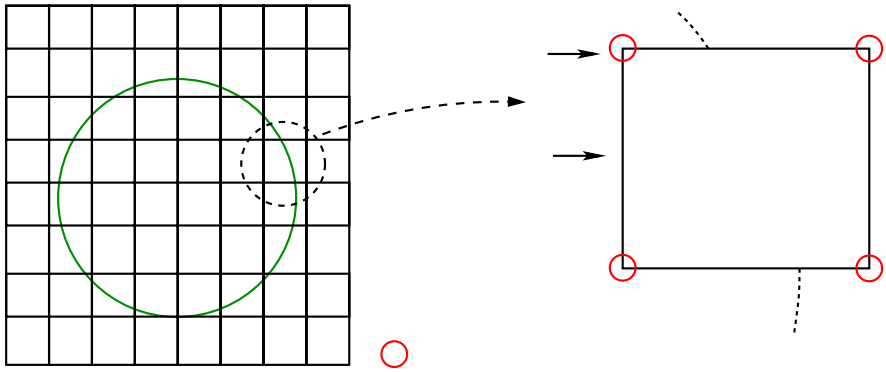

Fig. 2. Illustration of the Eulerian finite element mesh and the location of degrees of freedom on the mixed enriched finite element containing a segment of the interface. Circles show the location of bilinear element nodes and crosses show the location of biquadratic element nodes. The interface (green line) cutting through the element is represented implicitly using the level set function. (For interpretation of the references to color in this figure legend, the reader is referred to the web version of this article.)

and the Heaviside function H is defined as,

$$H(\mathbf{x},t) = \begin{cases} 1 & > 0, \\ 0 & < 0. \end{cases} \tag{25}$$

Note that the level set function is continuous across the interface and so that it can be interpolated using the shape functions N^I and N^Q.

Remark 5. Previously, Duddu et al. [2] proposed the above mixed formulation to ensure stability in the case of nearly incompressible elastic solids (e.g. rubber with Poisson's ratio $\nu = 0.48 - 0.5$). However, even for a compressible solid, the mixed formulation seems to yield better numerical accuracy and requires less number of iterations to reach the tolerance limit for the residual.

In this study, we reduce the dimension of the domain by considering that it is uniform in the x_3 direction (plane strain conditions apply). This implies that $u_3(\mathbf{x},t) = 0$; $F_{33}(\mathbf{x},t) = 1$; $F_{13}(\mathbf{x},t) = F_{32}(\mathbf{x},t) = 0$; this allows us to not

$$\text{shape functions } N_i = \begin{cases} N_V = N_V^{reg.}; N_V^{enr} & 2\ 36 \\ N_F = N_F^{reg.}; N_F^{enr} & 4\ 32 \\ N_J = N_J^{reg.}; N_J^{enr} & 1\ 8 \end{cases} \tag{28}$$

with

$$N_v^{reg} = N_v^1; \ldots; N_v^9 \quad {}_{2\ 18}; \qquad N_v^{enr} = S^1 N_v^1; \ldots; S^9 N_v^9 \quad {}_{2\ 18}$$

$$N_F^{reg} = N_F^1; \ldots; N_F^4 \quad {}_{4\ 16}; \qquad N_F^{enr} = S^1 N_F^1; \ldots; S^4 N_F^4 \quad {}_{4\ 16}$$

$$N_J^{reg} = N^1$$

$$y^{t+dt} = y^{t} + v^{?}.y^{t+dt/2}; t/dt + \bullet \quad v^{?}.y^{t+dt/2}; t/\frac{dt^2}{2}; \tag{36}$$

where $\bullet$ is the matrix of the angular velocity of the interface normal. Introducing the local coordinate axes $_1$ and $_2$ that respectively run in the directions tangent and normal to the interface at point y^{t}, the angular velocity can be written as,

$$! = v^{?} n_{; 1} z \quad \text{and} \quad _{ik} = _{ijk}!_{j} \tag{37}$$

with the permutation tensor $_{ijk} = \frac{1}{2}.i \quad j/. j \quad k/. k \quad i/$, indices $i; j; k = f1; 2; 3g$

Finally, a new level-set function $\phi(p; t + dt)$ can be calculated as the signed distance function at nodes p as follows [3]:

$$\phi(p; t + dt) = \operatorname{sgn}\left(\frac{y^{t+dt} - p}{|y^{t+dt} - p|} \cdot n_0^t\right) |y^{t+dt} - p|; \tag{44}$$

where y^{t+dt} is the particle associated with that time $t + dt$ and the "sgn" is the signum function. The reconstruction of the level set function using the local polynomial approximation of the interface is computationally inexpensive, and is used in the XFEM part of the algorithm. Let us summarize the GPM scheme in a pseudo algorithm as follows:

1. Given the initial level set function, find the coordinates of the particles that correspond to the nodes inside the computational tube (initialization step).
2. Given the velocity field v^t, update the position of the particle y^t to its current position y^{t+dt}.
3. For each particle y_0, find the neighboring particles to construct a local polynomial interpolation $\phi^{-1}(r^{-1}; t + dt)$ of the surface around y_0.
4. Given $r^{-1}(r^{-1}; t + dt)$, find the new particles by projecting the nodes inside the computational tube on the surface
5. Compute the new geometrical quantities such as the normal

$$w_F ; \; . \; \Omega C dt \quad \Omega \qquad D \; 0; \tag{50}$$

and the corresponding discretized forms are given by,

$$K_J^{enr} J_g^{enr} D \; R_J^{enr}; \tag{51}$$

$$K_F^{enr} F_g^{enr} D \; R_F^{enr}; \tag{52}$$

where J_g^{enr} and F_g^{enr} are the unknown global vectors of all enriched degrees of freedom; the global tangent matrices are given by,

$$K_J^{enr} D \sum_e \int_e N_J^{enr\,T} N_J^{enr} d \; e; \tag{53}$$

$$K_F^{enr} D \sum_e \int_e N_F^{enr\,T} N_F^{enr} d \; e I \tag{54}$$

and the residuals matrices are given by,

$$R_J^{enr} D \sum_e \int_e N_J^{enr\,T} \; J \Omega \; N_J^{reg} J^{reg} \; d \; e; \tag{55}$$

$$R_F^{enr} D \sum_e \int_e N_F^{enr\,T} \; F \Omega \; N_F^{reg} F^{reg} \; d \; e$$

Fig. 4. Schematic diagram of the uniaxial extension of a soft rectangular bar. A traction of 2 MPa is applied to the end of the bar to deform it elastically.

(a) Initial velocity variation in the domain.

(b) Velocity variation with depth after every 25 iterations.

1. Bilinear: 4-node FE interpolation of J; $\bar{F}$ & J
2. Biquadratic: 9-node FE interpolation of J; $\bar{F}$ & J
3. Mixed: 9-node FE interpolation of J and 4-node FE interpolation of $\bar{F}$ & J.

In the case of uniaxial extension in x_2, we have $J = F_{22} > 1$, since $F_{11} = F_{33} = 1$ and all other components of $\mathbf{F}$ vanish. Therefore, it is sufficient to only observe the behavior of F_{22} from $t = 0$ until equilibrium. In the following figures, we plot the variation of F_{22} in the x_2 direction every 50 iterations. Note that the length of the solid increases and the change in F_{22} decreases with each iteration as we approach equilibrium. We can see from Fig. 6 that for $\nu = 0$ the bilinear and mixed interpolation strategies work equally well, whereas the biquadratic interpolation strategy suffers from spurious oscillations close to the traction boundary. From Fig. 6 we can observe that for $\nu = 0.25$ both the bilinear and biquadratic interpolation strategies suffer from spurious oscillations, whereas the mixed interpolation strategy is least affected. This numerical example indicates that the mixed interpolation strategy leads to better accuracy and stability compared to the uniform interpolation strategies. However, the mathematics behind the superior performance of this mixed interpolation strategy for Eulerian solid mechanics in the compressible regime has not yet been fully investigated and will be the focus of a future study.

We next investigate the accuracy of the scheme by comparing the analytical and numerical equilibrium stress versus deformation curves. Using the constitutive law given in Eq. (15), we can derive the analytical expression for the Cauchy stress component σ_{22} as,

$$\sigma_{22} = \frac{1}{F_{22}} \left[\log(F_{22}) + \frac{2}{3} \left(F_{22}^{-2/3} \cdot F_{22}^{2} - 1 \right) \right] . \tag{58}$$

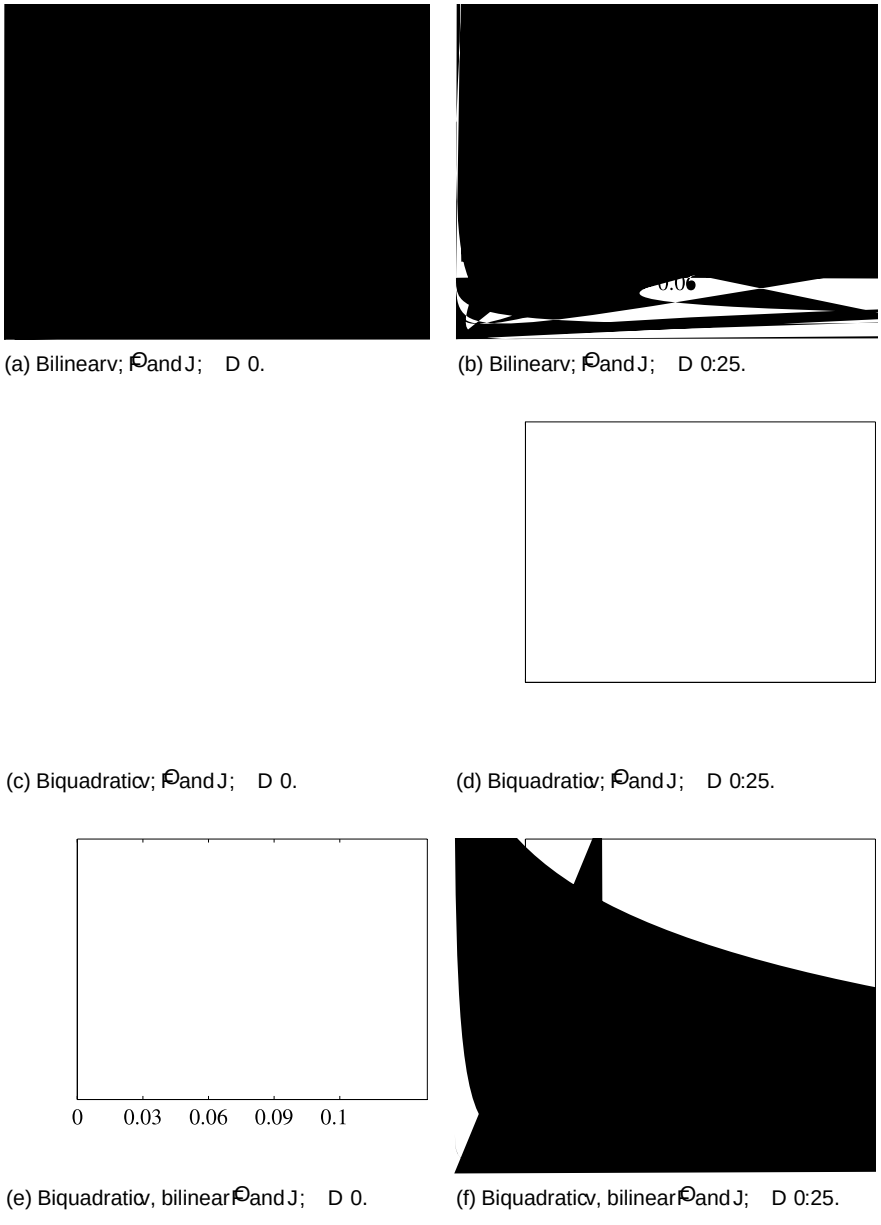

(a) Bilinear; $\bar{F}$ and J; $\nu = 0$.

(b) Bilinear; $\bar{F}$ and J; $\nu = 0.25$.

(c) Biquadratic; $\bar{F}$ and J; $\nu = 0$.

(d) Biquadratic; $\bar{F}$ and J; $\nu = 0.25$.

(e) Biquadratic, bilinear; $\bar{F}$ and J; $\nu = 0$.

(f) Biquadratic, bilinear; $\bar{F}$ and J; $\nu = 0.25$.

Fig. 6. Performance of the mixed element formulation for uniaxial tension test. Variation of F_{22} along the length of domain is shown for bilinear, biquadratic and mixed formulation for two compressible materials with Poisson's ratio $\nu = 0$ (left column) and $\nu = 0.25$ (right column).

right to left as shown in Fig. 8(a), so the velocity is negative. In the case of simple shear x direction, we have $F_{12} > 0$; $F_{22} = F_{11} = F_{33} = 1$ and all other components of $\mathbf{F}$ are zero. Therefore, it is sufficient to only observe the behavior of F_{12} from $t = 0$ until equilibrium. We next plot the match between the analytical and numerical curves for equilibrium stress versus deformation. From the constitutive relation in Eq. (15), we can write the analytical expression for the Cauchy stress component $\sigma_{12} = F_{12}$. For four different values of applied shear stress, we plot the numerical results (scatter) against the analytical solution (solid line) in Fig. 8(b). We observe an excellent agreement between theory and simulation with a linear response in the applied stress range. Since

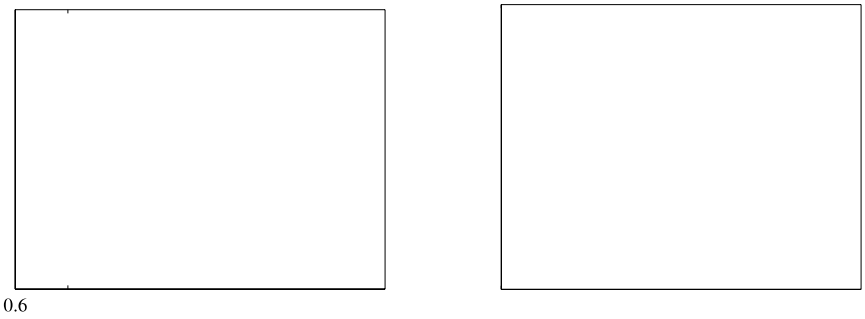

(a) Analytical and numerical curves for stress versus deformation gradient.

(b) Percentage error in elastic body mass with pseudo time (iteration) steps.

Fig. 7. Validation and error analysis of numerical results from the CEL formulation for uniaxial tension test.

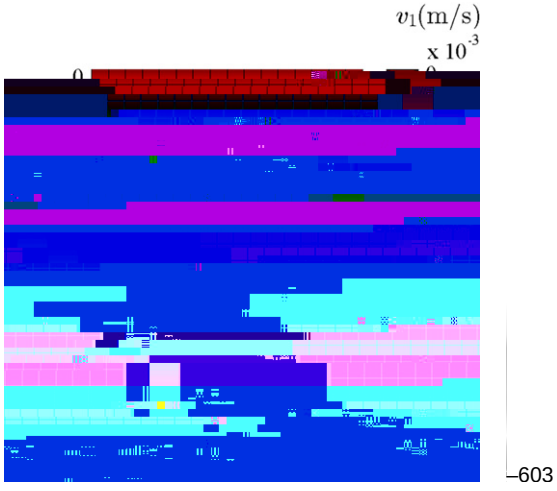

(a) Initial velocity variation in the domain.

(b) Analytical and numerical curves for stress versus deformation gradient.

Fig. 8. Numerical results from the CEL formulation for the shear flow of material under applied shear traction. The results are in agreement with theory, thus, validating our scheme.

4.3. Indentation of a rounded rectangular solid

Let us consider a rounded rectangular solid made up of the same soft material as in the previous example (E_Y D 15:0 MPa and D 0:25). The dimensions of the straight portion of the rounded rectangle is 3 0:92 cm and the rounded edges are semicircles with radius 0.46 cm. The solid domain and test configuration are chosen to mimic a hydrogel placed onto a relatively rigid substratum, typically seen in tissue printing. The total computational domain is 2 cm 1:2 cm that is discretized using an element size 0:1 cm. Note that the computational domain

Fig. 9. Schematic diagram of the indentation of soft solid. A Gaussian type pressure load is applied to simulate the contact between a rigid indente

Table 1
Percentage error in elastic body mass for different finite element mesh sizes for the deforming cylinder under lateral compression at equilibrium.

Element size	Element in X-dir	Element in Y-dir	% Error
0.16	40	30	1.6
0.08	80	60	0.28
0.04	160	120	0.16

4.4. Lateral compression of a cylinder

In the previous two benchmark examples, the interface remained flat at all times. Herein, we shall consider an example problem with a curved interface and demonstrate the ability of our formulation to handle its evolution as the solid undergoes very large deformation. Let us consider an elastic compressible cylinder of radius $R = 0.81$ cm, with $E_Y = 15.0$ MPa and $\nu = 0.25$, which is compressed between two planes on the top and bottom. The total computational domain is 2 cm $\times$ 2.4 cm that is discretized using an element size $h = 0.08$ cm. Plane strain conditions apply and body forces are neglected. We set up the problem with four-fold symmetry about the origin. The boundary and initial conditions for this problem are,

$$\left.\begin{array}{l} v_2(x_1,\ x_2 = 0) = 0 \ \text{and} \ v_1(x_1 = 0,\ x_2) = 0, \\ \boldsymbol{v}(\boldsymbol{x},\ t = 0) = \boldsymbol{0}, \\ p(\boldsymbol{x},\ t = 0) = 1, \\ J(\boldsymbol{x},\ t = 0) = 1. \end{array}\right\} \tag{62}$$

We define a vertical force that is applied on the portion of interface, Γ_t. This force function is defined as an exponential repulsive force to avoid penetration between the cylinder and the two compressive planes:

$$\boldsymbol{t}(\boldsymbol{x}) = \begin{cases} (x - d_0)\exp(d_0 - x)\boldsymbol{e}_2 & \text{if } x \le d_0 \\ \boldsymbol{0} & x > d_0 \end{cases}.$$

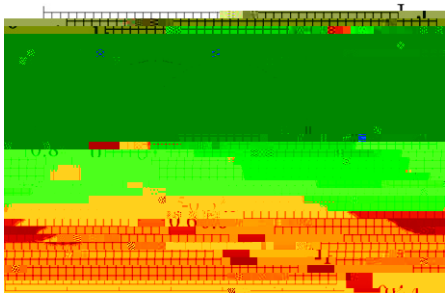

(a) Initial interface at iteration D 0.

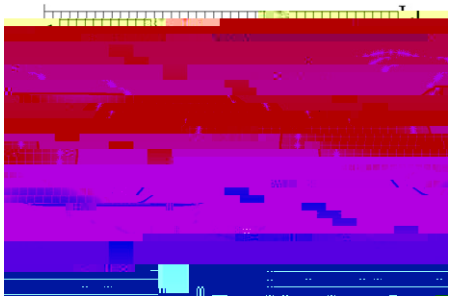

(b) Deformed interface at iteration D 25.

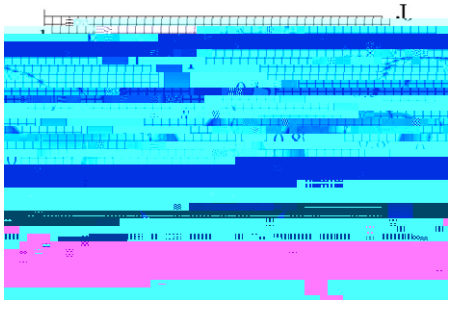

(c) Deformed interface at iteration D 50.

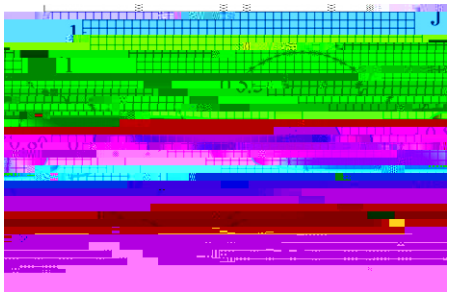

(d) Deformed interface at iteration D 112.

$$N_{F3} = \begin{bmatrix} 0 & 0 & N_1 & 0 \\ 0 & 0 & 0 & N_1 \\ 0 & 0 & N_2 & 0 \\ 0 & 0 & 0 & N_2 \end{bmatrix}_{4\times 4} \qquad N_{F4} = \begin{bmatrix} 0 & 0 & 0 & 0 \\ 0 & 0 & 0 & N_2 \\ 0 & 0 & 0 & 0 \\ 0 & 0 & 0 & N_1 \end{bmatrix}_{4\times 4} :$$

References

[1] D. Demarco, E.N. Dvorkin, An Eulerian nite element formulation for modelling stationary nite strain elastic deformation processes, Internat. J. Numer. Methods Engrg. 62 (8) (2005) 1038–1063.

[2] R. Duddu, L.L. Lavier, T.J.R. Hughes, V.M. Calo, A nite strain Eulerian formulation for compressible and nearly incompressible hyper-elasticity using high-order B-spline nite elements, Internat. J. Numer. Methods Engrg. 89 (6) (2012) 762–785.

[3] S. Leung, H. z0(S.)-2(.)-332(La)2 6ALaal.base250(al.par(uslents,)-m(Engrnts,)-mpress,)-mo283Jf37((acents,)-]TJ5(ymernat.)-er)55(.)0(Metl

[29] E. Béchet, N. Moës, B. Wohlmuth, A stable Lagrange multiplier space for stiff interface conditions within the extended finite element method, Internat. J. Numer. Methods Engrg. 78 (8) (2009) 931–954.
[30] T.-Y. Kim, J. Dolbow, T. Laursen, A mortared finite element method for frictional contact on arbitrary interfaces, Comput. Mech. 39 (3) (2007) 223–235.
[31] J. Dolbow, I. Harari, An efficient finite element method for embedded interface problems, Internat. J. Numer. Methods Engrg. 78 (2) (2009) 229–252.
[32] C. Annavarapu, M. Hautefeuille, J.E. Dolbow, A robust Nitsche's formulation for interface problems, Comput. Methods Appl. Mech. Engrg. 225–228 (2012) 44–54.
[33]